Naval Research Laboratory
Washington, DC 20375-5320

U.S. NAVAL RESEARCH LABORATORY

NRL/5340/MR—2023/6

Generative Models for Monostatic K-Space Enrichment

HATIM F. ALQADAH

MATTHEW J. BURFEINDT

Advanced Signal Processing Section
Surveillance Technology Division
Radar Division

RAGHU G. RAJ

Radar Imaging and Target ID Section
Radar Analysis Branch
Radar Division

November 13, 2023

REPORT DOCUMENTATION PAGE

Form Approved
OMB No. 0704-0188

1. REPORT DATE *(DD-MM-YYYY)*	**2. REPORT TYPE**	**3. DATES COVERED** *(From - To)*
13-11-2023	NRL Memorandum Report	01 October 2022 – 30 September 2023

4. TITLE AND SUBTITLE

Generative Models for Monostatic K-Space Enrichment

5a. CONTRACT NUMBER

5b. GRANT NUMBER

5c. PROGRAM ELEMENT NUMBER
61553N

6. AUTHOR(S)

Hatim F. Alqadah, Matthew J. Burfeindt, and Raghu G. Raj

5d. PROJECT NUMBER

5e. TASK NUMBER

5f. WORK UNIT NUMBER
1Y36

7. PERFORMING ORGANIZATION NAME(S) AND ADDRESS(ES)

Naval Research Laboratory
4555 Overlook Avenue, SW
Washington, DC 20375-5320

8. PERFORMING ORGANIZATION REPORT NUMBER

NRL/5340/MR--2023/6

9. SPONSORING / MONITORING AGENCY NAME(S) AND ADDRESS(ES)

Office of Naval Research
One Liberty Center
875 N. Randolph Street, Suite 1425
Arlington, VA 22203-1995

10. SPONSOR / MONITOR'S ACRONYM(S)

ONR

11. SPONSOR / MONITOR'S REPORT NUMBER(S)

12. DISTRIBUTION / AVAILABILITY STATEMENT

DISTRIBUTION STATEMENT A: Approved for public release; distribution is unlimited.

13. SUPPLEMENTARY NOTES

14. ABSTRACT

We provide a summary of our investigation regarding K-space augmentation algorithms based on the use of deep generative models for enhancing monostatic radar synthetic aperture imaging. The approach is based on incorporating contextual generative priors into the relevant inverse problem when restricted to a known class of targets. Initial training performance of the generative models as well as efficacy of the proposed contexutual generative approach is presented.

15. SUBJECT TERMS

Radar imaging — Generative networks — DNN
Inverse scattering — Backprojection — K-space augmentation

16. SECURITY CLASSIFICATION OF:			**17. LIMITATION OF ABSTRACT**	**18. NUMBER OF PAGES**	**19a. NAME OF RESPONSIBLE PERSON**
a. REPORT	**b. ABSTRACT**	**c. THIS PAGE**			Hatim Alqadah
U	U	U	U	16	**19b. TELEPHONE NUMBER** *(include area code)* (202) 404-8106

Standard Form 298 (Rev. 8-98)
Prescribed by ANSI Std. Z39.18

This page intentionally left blank.

CONTENTS

FIGURES

EXECUTIVE SUMMARY

The work discussed in this report is part of an overall research program (WU 1Y36, FY22-FY24, PI: Raj) which is focused on the use of machine learning and in particular generative methods to enhance radar imaging performance under reduced spatio-temporal-spectral diversity scenarios. Here we report on the incorporation of a novel contextual Generative Adversarial Networks (GAN) algorithm within a backprojection imaging framework. The proposed contextual GAN algorithms aims to provide a means of completing missing spatial frequency (K-space) information in a manner that is both physically relevant and consistent with the actual scattered electromagnetic field measurements observed for a particular scene. During FY23 developments were undertaken to provide initial proof of concept of the proposed algorithms. Specifically the following accomplishments were made:

- Construction of relatively large-scale training sets using computational electromagnetic simulations for simple target classes.
- Design of appropriate Deep Neural Network (DNN) architectures for both a generative and discrimination networks.
- Develop an appropriate training framework for the proposed GAN.
- Develop a concrete optimization framework for a K-space completion algorithm that exploits the trained GANs
- Provide initial proof of concept of the completion algorithms against simple target structures using simulated electromagnetic measurements.

This page intentionally left blank

APPLICATION OF GENERATIVE MODELS FOR MONOSTATIC K-SPACE ENRICHMENT

1. MOTIVATION AND OBJECTIVE

Achieving robust target recognition for radar imaging modalities such as synthetic aperture radar (SAR) and inverse synthetic aperture radar (ISAR) still remains a challenge. Much of the difficulties for target recognition is due to the fact that the appearance and geometric distortions of targets can vary wildly in response to changes in bistatic geometry, background/clutter interactions, and other factors. Furthermore, unwanted image artifacts due to sidelobe interference and/or multiple scattering also have a detrimental effect on target detection and classification efforts. As such, ensuring a more stable image reconstruction process is key for improving radar perception capabilities. SAR and ISAR imaging are special cases of a mathematical problem known as inverse scattering, where the goal is to recover an image given knowledge of the scattered electromagnetic field. Unfortunately, inverse scattering is essentially a non-unique problem in the sense that in the presence of small perturbations in the scatter data, a number of different and highly dissimilar images can provide a good fit to the measurements. To help reduce ambiguities, over-redundant measurements in K-space is paramount to ensure that a physically-relevant image is computed. As briefly discussed in this report, a high degree of K-space diversity can be achieved through a combination of wide band waveforms and/or wide-angle multistatic geometries. While such configurations help to provide extensive K-space coverage, they are usually not feasible due to cost or operational constraints. Narrow band monostatic radar geometries are far more cost effective and simpler to implement/deploy but yield limited K-space diversity.

The goal of this work is to investigate a means for augmenting SAR and/or ISAR monostatic measurements with physically relevant virtual data generated by predictive algorithms. A theoretical basis for achieving K-space augmentation lies in the fact that, under reasonable regularity conditions on the underlying scatterers, the resulting scattering amplitude is real analytic with respect to space and frequency [1, 2]. As such, whenever the scattering amplitude is known on a continuous subset of a given region Ω_B in K-space, a unique extension onto Ω_B exists. Unfortunately the augmentation problem, similar to the inverse scattering problem, is itself a highly ill-posed one. As such, in the absence of suitable prior knowledge on the underlying solution, achieving a physically relevant solution to the augmentation problem is numerically challenging. Prior studies have proposed various augmentation algorithms based on classical stability priors such as Tikhonov regularization [3] and total-variation (TV) [4], and more recently those based on low-rank matrix priors [5]. All of these methods however, can be thought of as blind techniques which do not adapt from prior observed data.

Deep learning (DL) and in particular generative artificial intelligence (AI) have been shown to be very effective means for learning prior data distributions and the various patterns within them. Generative AI has been successfully incorporated for data augmentation problems in similar areas such as image completion [6] from missing/corrupted pixel data and super-resolution problems [7], where the goal is to recover a high resolution image from a low resolution measurement. To our knowledge, generative AI has not yet been adopted for radar image reconstruction and augmentation. The work undertaken here is an initial attempt

Manuscript approved November 7, 2023.

towards applying generative AI to the K-space augmentation problem. Specifically the main goals of this work were:

1. To train generative models to synthesize realistic K-space data for certain scenes or target classes.
2. Complete limited K-space measurements yielded by monostatic geometries using trained generative models.

The ability to generate realistic K-space scatter data is a essentially a means of computing the radar cross section (RCS) for random but physically relevant targets/scenes which naturally has a number of beneficial applications besides the K-space augmentation problem. The second objective is to exploit a generative model by putting synthetic K-space data in context with given monostatic measurements. The approach undertaken in FY23 relied on the use of a GAN which is a generative model based on a game-theoretic approach for training. One of the main advantages of using a GAN here was the ability to achieve model convergence from relatively small training data sets. This is a very important feature with respect to radar-focused machine learning and AI applications, since appropriate radar training data is highly sparse as compared to other ML/AI driven fields such as computer vision.

2. BACKGROUND

We consider propagation and scattering in two-dimensional Euclidean space. The unknown scene is characterized by a reflectivity function $\rho(\mathbf{x})$, which is assumed to be of compact support embedded in free space. The radar transmits a signal of bandwidth $B := [f_{\min}, f_{\max}]$, which we assume is sufficiently in the far-field and impinges on the target(s) in the form of a plane wave propagating in the direction $\hat{\mathbf{d}}$. For a fixed frequency ω the observed scattered electric field $E^{sc}(\mathbf{x})$ satisfies the forward Helmholtz model

$$\nabla^2 E^{\text{total}}(\mathbf{x}) + k^2(1-\rho(\mathbf{x}))E^{\text{total}} = 0 \tag{1}$$

$$E^{\text{total}}(\mathbf{x}) = E^{\text{sc}}(\mathbf{x}) + E^{\text{inc}}(\mathbf{x}) \tag{2}$$

$$\lim_{R\to\infty} \sqrt{R}\left(\frac{\partial E^{\text{sc}}}{\partial R} - ikE^{\text{sc}}\right) = 0,\ \mathbf{x} = R\hat{\mathbf{x}}., \tag{3}$$

where $k = \omega/c_0$ is the wavenumber. The scattered field satisfying equations (1)-(3) can be represented in integral form as

$$E^{\text{sc}}(\mathbf{x}) = k^2 \int G(\mathbf{x},\mathbf{y})\rho(\mathbf{y})E^{\text{total}}(\mathbf{y})d\mathbf{y}, \tag{4}$$

where $G(\cdot,\cdot)$ is the free space Green's function

$$G(\mathbf{x},\mathbf{y}) = \frac{i}{4}H_0^1(k|\mathbf{x}-\mathbf{y}|). \tag{5}$$

At an observation point $\mathbf{x}$ located in the far-field zone, the scattered field can be approximated as

$$E^{\text{sc}}(\mathbf{x}) \approx \frac{e^{ikR}}{\sqrt{R}} E_\infty^{\text{sc}}(\hat{\mathbf{x}};\hat{\mathbf{d}},\omega), \tag{6}$$

where the scattering amplitude $E_\infty^{\text{sc}}(\hat{\mathbf{x}}; \hat{\mathbf{d}}, \omega)$ is given as

$$E_\infty^{\text{sc}}(\hat{\mathbf{x}}; \hat{\mathbf{d}}, \omega) = k^2 \int e^{-ik\hat{\mathbf{x}}\cdot\mathbf{y}} \rho(\mathbf{y}) E^{\text{total}}(\mathbf{y}) d\mathbf{y}. \tag{7}$$

The scattering amplitude encapsulates all the information available for reconstructing the target ρ and is a function of the bistatic geometry and frequency band.

2.1 Born Approximation and K-Space Model

Note that (7) actually defines a non-linear relationship between the scattering amplitude and the underlying image, since the total-field itself depends on $\rho(\cdot)$. To yield a linear relationship between the scattering amplitude and the image we can assume that the Born approximation holds, which presumes that the total field is dominated by the incident field. In which case, for plane wave incidence equation (7) reduces to

$$E_\infty^{\text{sc}}(\hat{\mathbf{x}}; \hat{\mathbf{d}}, \omega) = k^2 \int e^{-ik(\hat{\mathbf{x}}-\mathbf{d})\cdot\mathbf{y}} \rho(\mathbf{y}) d\mathbf{y}. \tag{8}$$

The linear model (8) is in the form of a Fourier transform where the spatial frequencies (knots) $\mathbf{K}$ are given as

$$\mathbf{K} = k(\hat{\mathbf{x}} - \hat{\mathbf{d}}). \tag{9}$$

The image of the scene can thus be recovered via the backprojection

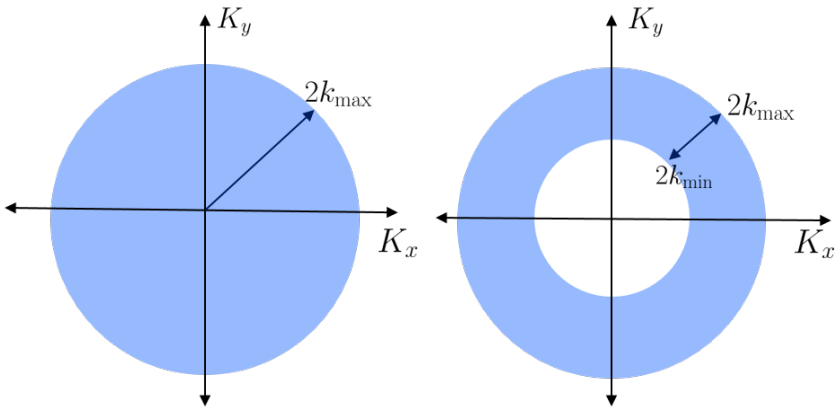

(a) Full K-space support (b) Monostatic K-space support

Fig. 1—For a given bandwidth, complete K-space information is contained in the disk region. Multistatic geometries over-sample the complete region whereas monostatic geometries only sample the higher spatial frequencies.

$$I(\mathbf{x}) = \int E_\infty^{\text{sc}}(\mathbf{K}) e^{i\mathbf{K}\cdot\mathbf{x}} d\mathbf{K}. \tag{10}$$

For a given bistatic geometry and fixed frequency, the knots lie on a circle centered at $k\hat{\mathbf{d}}$ with radius k. For the case of a monostatic geometry, where $\hat{\mathbf{x}} = -\hat{\mathbf{d}}$, the knots reduce to

$$\mathbf{K}_{\text{monostatic}} = 2k\hat{\mathbf{x}}, \tag{11}$$

which for a fixed frequency defines a circle of radius $2k$ centered at the origin. As shown in Figure 1, the scattering amplitude given on a band $B = [f_{\min}, f_{\max}]$ and measured with a complete multistatic geometry samples the disk region Ω_B in K-space. Whereas a full aperture monostatic geometry only samples an annular region in K-space. Therfore in the monostatic case, even under full aperture conditions, only the higher spatial frequencies are used in the inversion which leads to a number of stability problems especially in narrow band scenarios. Limited aperture geometries also has the effect of reducing cross-range resolution in the image.

3. LEARNING RELEVANT K-SPACE SURFACES VIA GENERATIVE NETWORKS

An investigation focused on the use of GANs to synthesize complete and physically relevant K-space data in Ω_B for certain target classes was conducted. GANs cast the learning problem as a game between two DNNs, the generator G, which defines a mapping between a latent space and the K-space data, and the discriminator D, which attempts to classify given K-space data as either synthetically generated or as a true measurement. The two models are trained simultaneously with respect to known prior data until the two networks achieve some sort of equilibrium. The objective is to get the generator to a state where it can produce highly realistic data. A standard GAN approach [8] optimizes the network parameters of G and D against the min-max loss function

$$\min_G \max_D \mathbb{E}_{\mathbf{U}\sim\mathbb{P}_r}\left[\log(D(\mathbf{U}))\right] + \mathbb{E}_{\mathbf{z}\sim\mathbb{P}_g}\left[\log(1 - D(G(\mathbf{z}))\right], \tag{12}$$

where $\mathbb{E}_{\mathbf{U}\sim\mathbb{P}_r}[\cdot]$ denotes the expectation operator with respect to the true data probability distribution and $\mathbb{E}_{\mathbf{z}\sim\mathbb{P}_g}[\cdot]$ is the expectation operator with respect to the latent distribution $\mathbb{P}_g$. Unfortunately, in our numerical experiments, we found this approach to be rather unstable as the resulting GAN exhibited what is known as *mode collapse* [9]; a form of training instability in which the generator synthesizes essentially the same output regardless of the input latent vector. Alternative loss functions that seek to mitigate this issue can be found in the literature. One particular approach that we found to be effective was based on the Wasserstein-1 loss [10]

$$\min_G \max_{D\in\mathcal{L}} \mathbb{E}_{\mathbf{U}\sim\mathbb{P}_r}\left[D(\mathbf{U})\right] - \mathbb{E}_{\tilde{\mathbf{U}}\sim\mathbb{P}_g}\left[\, D(\tilde{\mathbf{U}})\right], \tag{13}$$

where $\mathcal{L}$ is the set of 1-Lipschitz continuous functions and $\tilde{\mathbf{U}} = G(\mathbf{z})$. To enforce the Lipschitz continuity constraint on the discriminator we augment the discriminator loss function with a gradient penalty regularization term [11]. Therefore the complete loss function for training the discriminator can be explicitly written as

$$L(D) = \mathbb{E}_{\tilde{\mathbf{U}}\sim\mathbb{P}_g}\left[\, D(\tilde{\mathbf{U}})\right] - \mathbb{E}_{\mathbf{U}\sim\mathbb{P}_r}\left[D(\mathbf{U})\right] + \alpha\mathbb{E}_{\hat{\mathbf{U}}\sim\mathbb{P}_d}\left[\|\nabla_{\hat{\mathbf{U}}}(\|D(\hat{\mathbf{U}})\|_2 - 1)^2\right]. \tag{14}$$

Samples of the distribution $\mathbb{P}_d$ are those that are drawn along lines between pairs of points from the $\mathbb{P}_r$ and $\mathbb{P}_g$ distributions.

3.1 Proposed GAN Training Framework

Our proposed training framework is summarized in Figure 2 and is based on the assumption that we have a training set comprised of scenes measured with complete K-space data in Ω_B. In this work we constructed

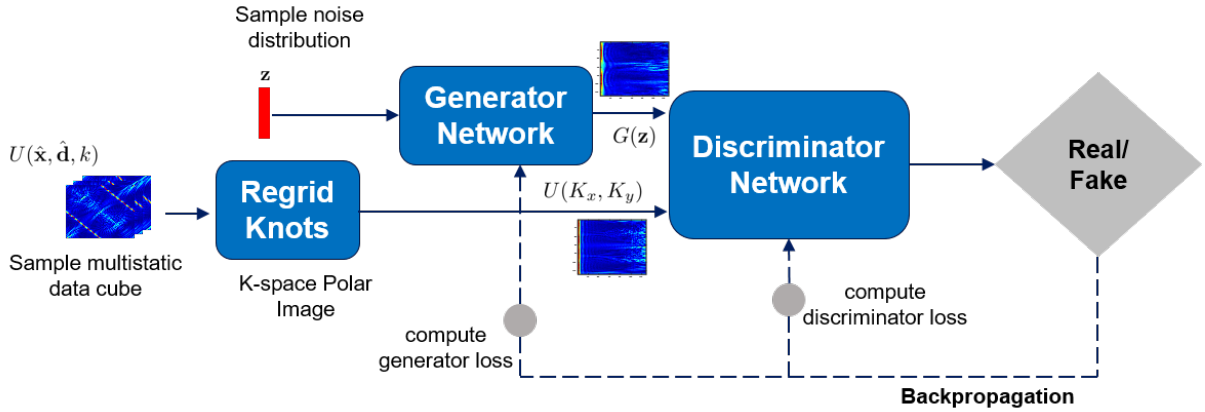

Fig. 2—Adversarial training approach for learning K-space surfaces. Multistatic data cubes are processed to yield K-space samples on a regular polar grid. The resulting polar complex images are supplied to the discriminator to learn the difference between generated K-space surfaces and measured ones.

complete K-space data sets via dense multistatic geometries. For the case where training data is obtained numerical via electromagnetic (EM) simulation, multistatic geometries are easy to incorporate, and based on recent works, it appears that complex numerical EM models are actually effective for training DL models for real-world deployment [12]. On the other hand, for more complex scenes or targets that cannot be modeled via simulation, training data should be obtained via *measured data*, in which case using dense multistatic measurements may be challenging. However, as shown in Figure 1, an alternative way to get almost complete K-space data would be to use wide band monostatic geometries for measured data.

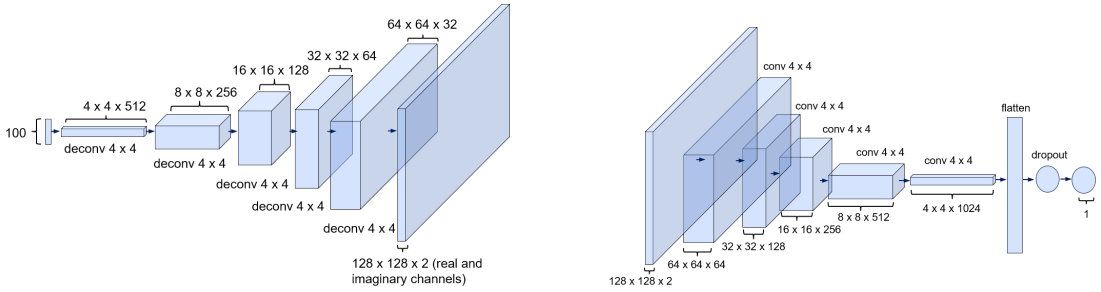

(a) Generator (b) Discriminator

Fig. 3—Illustrating the deep convolutional network architectures for the generator and the discriminator.

It is important to note that most DNN architectures appropriate for the generator G, as well as the discriminator D, are based on tensors that assume a regular grid in Cartesian space. K-space images however

are polar, i.e., the pixels lie on a regular *polar grid* and are not suitable for conventional DNN architectures. Thus our training procedure incorporates an interpolation stage which effectively unwraps the K-space data onto a regular Cartesian grid. The disadvantage of this approach however is that the periodicity of the data is lost. One potential solution to this (which we did not incorporate here) is to use a Fourier network [13] layer in the generator's architecture. As discussed in [13], a Fourier layer given as the first layer in any network ensures that the resulting output will be periodic with respect to its input parameters. Future work of ours will seek architectures that incorporate this. In any case, the specific architectures used for the generator and discriminator in this work are shown in Figure 3. The generator shown here draws a 100×1 vector from a standard Normal distribution and then undergoes a number of transpose convolutional layers to yield $\mathbf{U}$ which is a $128 \times 128 \times 2$ image with the real and imaginary values stacked as separate channels. The discriminator takes a K-space image $\mathbf{U}$ as input and maps it to a scalar in the range of $[-\infty, \infty]$ which is used as a likelihood score to indicate whether or not a given K-space image is real (physical).

3.2 A Contextual Generative Predictive Algorithm

Initial development of augmentation algorithms that exploit trained generative models for augmenting sampled monostatic data was undertaken in FY23. The developed algorithms are based on an optimization framework that is tasked to find an appropriate vector $\hat{\mathbf{z}}$ in the latent space that maps to a K-space image that best matches the known monostatic measurements. The framework is succinctly described as:

$$\hat{\mathbf{z}} = \arg\min_{\mathbf{z}\sim\mathbb{P}_{\mathbf{z}}} \left\{ \mathcal{L}_c(\mathbf{z}|\mathbf{y}, \mathbf{M}) + \beta \mathcal{L}_p(\mathbf{z}) \right\}. \tag{15}$$

Here the term $\mathcal{L}_c(\cdot)$ refers to the contextual loss which seeks to penalize latent solutions that deviate from the known measurements. The second term $\mathcal{L}_p(\cdot)$ is a regularization term that will penalize unrealistic solutions as dictated by the discriminator and is weighted by the scalar $\beta > 0$. The quantity $\mathbf{M}$ is a binary mask being the same size as $\mathbf{U}$ which has ones for the indices where the monostatic spatial frequencies are known and zeros otherwise. In this work we used considered an ℓ_1 proximity term for the contextual loss

$$\mathcal{L}_c(\mathbf{z}|\mathbf{Y}, \mathbf{M}) = \|\mathbf{W} \odot (G(\mathbf{z}) - \mathbf{Y})\|_1, \tag{16}$$

where $\mathbf{W}$ is a weighted mask defined as

$$\mathbf{W} = \begin{cases} \sum_{j \in N(i)} \frac{(1-M_j)}{|N(i)|} & \text{if } \mathbf{M}_i \neq 0 \\ 0 & \text{if } \mathbf{M}_i = 0 \end{cases}, \tag{17}$$

where i indexes a pixel location of $\mathbf{U}$ and $N(i)$ is pre-defined neighborhood of pixel i, and $|\cdot|$ in this context denotes cardinality. For the prior loss we opt to use a weighted response of the discriminator:

$$\mathcal{L}_p(\mathbf{z}) = -D(G(\mathbf{z})). \tag{18}$$

4. SIMULATION RESULTS

Simulation work undertaken in FY23 aimed to demonstrate proof of concept of the proposed generative models as well as the contextual augmentation approach. Efforts were dedicated towards constructing

appropriate training data sets of complete K-space data for various target classes composed of simple target models. For this we leveraged computational EM codes to simulate the actual scattered fields. As computational speed is an important factor for constructing large-scale data sets, we used a frequency domain Method of Moments (MOM) solver for dense multistatic data computed on narrow bands. For wide bandwidths, we used a Finite-Difference Time Domain (FDTD) method to generate the scattered field of the underlying targets. A large-scale set of two-dimensional random conducting polygonal targets simulated at 1 GHz using a 1 MHz bandwidth was constructed via the MOM solver. Furthermore, approximately 1000 conducting targets based on the MNIST digits [14] data set were also simulated at 1 GHz using a 300 MHz bandwidth. Simulations with the MNIST data set are currently on-going and will be analyzed further in FY24.

4.1 GAN Training with Polygonal Targets

In FY23 we mostly worked with the polygonal data set as an initial proof point. We note that prior to training we corrupted all scattering amplitude data with Gaussian noise using a 40 dB signal-to-noise ratio (SNR). Training was conducted using the TensorFlow computational framework on a workstation equipped with 128 GB of memory and a NVIDIA Titan V GPU. Training for the polygon data set took approximately 1.5 hours to conduct. Figure 4 shows the evolution of the discriminator loss function during training and its convergence towards equilibrium. Visual comparisons between the K-space images generated by the EM

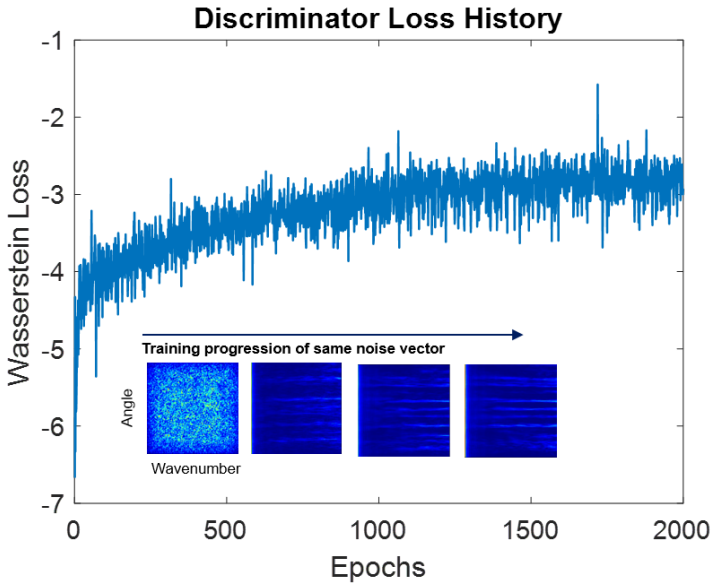

Fig. 4—Illustrating discriminator loss as a function of training epochs as well as the evolution of a single noise vector mapped to its respective K-space image as training progresses.

solver and those generated by the GAN were used as an initial validation of the GAN's efficacy, an example of which is shown Figure 5. We can visually observe that prominent K-space features between the two are quite similar. Visual inspections between the backprojected K-space surfaces between the two sources were also conducted. An example comparison is shown in Figure 6. We see that the GAN was quite successful of producing backprojections of various random polygonal targets whose appearance matches what we would expect.

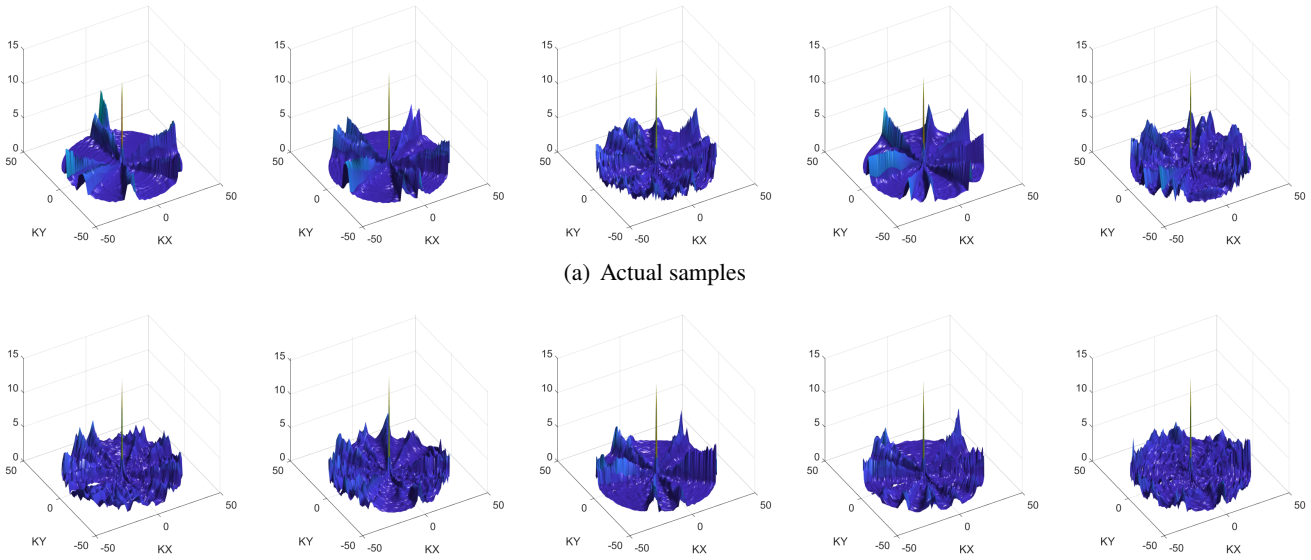

(a) Actual samples

(b) GAN outputs

Fig. 5—Showing magnitude K-space plots obtained via computational electromagnetic simulation (top) as well as samples obtained via the trained GAN. The surfaces generated by the GAN exhibited similar features contained in the true K-space surface in both the high and low frequency regions.

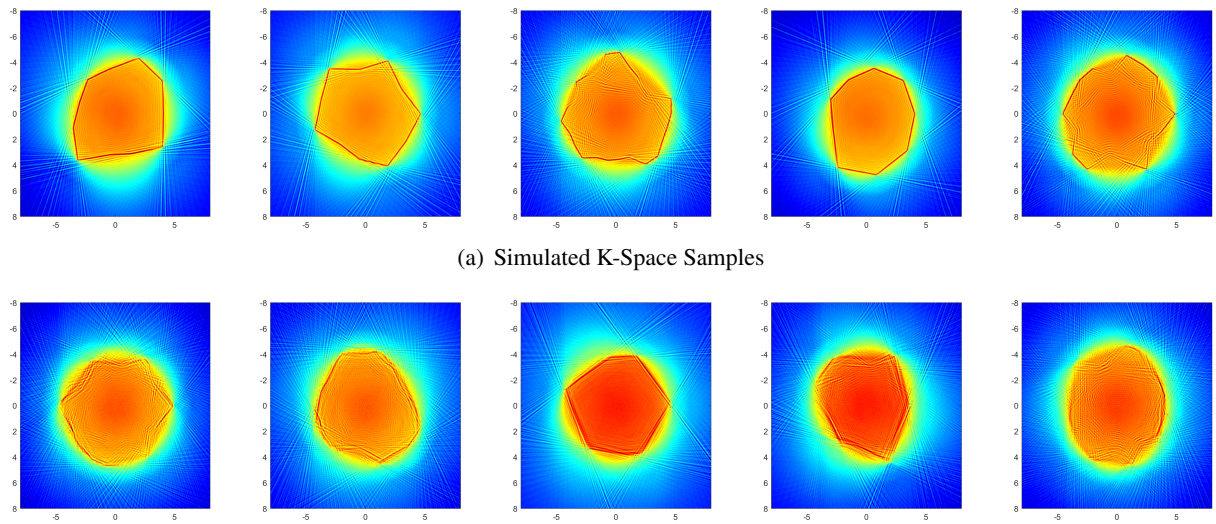

(a) Simulated K-Space Samples

(b) Fake K-Space Samples

Fig. 6—Fourier backprojection results for actual and synthetic K-space surfaces.

4.2 Monostatic Augmentation with Polygon Targets

Initial evaluations of the proposed augmentation framework were conducted using monostatic data for additional polygonal targets not contained in the initial training data set. The monostatic data was generated using the MOM solver and was corrupted with additive white noise at a 20 dB SNR. Note the SNR used here was chosen to be lower than what was used in training since in real-world scenarios the measured data would naturally be noisier than data obtained in a training environment. The proposed completion program

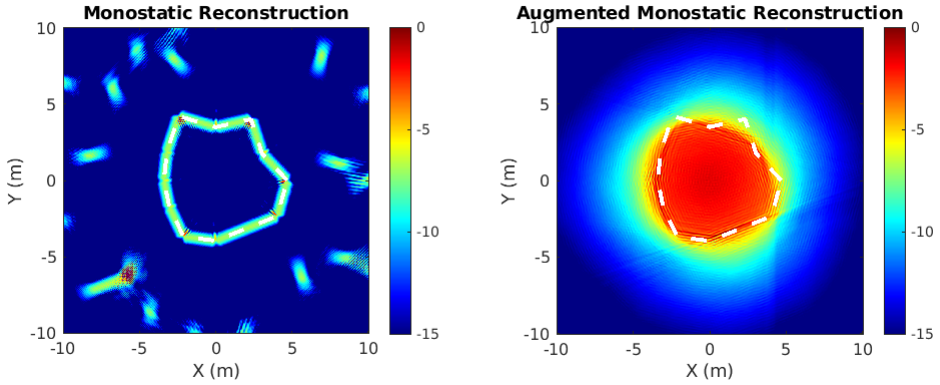

(a)

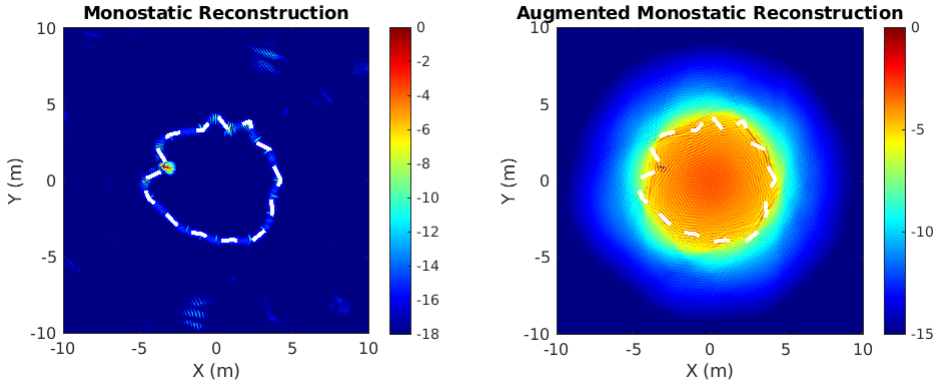

(b)

Fig. 7—Backprojection reconstruction using monostatic and augmented monostatic K-space data. The dashed lines indicated the true boundary of the targets.

in (15) was minimized via gradient descent in TensorFlow. Example results are shown in 7. We observe here that although scattering centers are resolved along the target boundaries in the monostatic reconstructions, strong scatterers are apparent in the exterior regions. However in the augmented reconstructions those false scatterers are effectively eliminated and a more faithful reconstruction of the target geometry is obtained. Simulations with more complex target structures will be undertaken during FY24.

REFERENCES

1. R. Griesmaier, N. Hyvönen, and O. Seiskari, "A note on analyticity properties of far field patterns" (2013), ISSN 1930-8337, URL /article/id/875e9476-8a6e-4918-b20b-0fc9779f846b.

2. D. Colton and R. Kress, *Inverse Acoustic and Electromagnetic Scattering Theory* (Springer, 1998).

3. R. Djellouli, R. Tezaur, and C. Farhat, "On the solution of inverse obstacle acoustic scattering problems with a limited aperture," in G. C. Cohen, P. Joly, E. Heikkola, and P. Neittaanmäki, eds., *Mathematical and Numerical Aspects of Wave Propagation WAVES 2003*, pp. 625–630, Berlin, Heidelberg, 2003 (Springer Berlin Heidelberg), ISBN 978-3-642-55856-6.

4. A. Barucq, C. Bekley, and R. Djellouli, "A multi-step procedure for enriching limited two-dimensional acoustic far-field pattern measurements," *Journal of Inverse and Ill-posed Problems* **18**, 189–216 (2010).

5. H. F. Alqadah and M. Burfeindt, "A far-field transformation procedure for monostatic linear sampling method imaging," in *2019 International Conference on Electromagnetics in Advanced Applications (ICEAA)*, pp. 1387–1392 (2019), doi:10.1109/ICEAA.2019.8879380.

6. R. A. Yeh, C. Chen, T. Lim, A. G. Schwing, M. Hasegawa-Johnson, and M. N. Do, "Semantic image inpainting with deep generative models," in *2017 IEEE Conference on Computer Vision and Pattern Recognition (CVPR)*, pp. 6882–6890, Los Alamitos, CA, USA, jul 2017 (IEEE Computer Society), doi:10.1109/CVPR.2017.728, URL https://doi.ieeecomputersociety.org/10.1109/CVPR.2017.728.

7. C. Ledig, L. Theis, F. Huszar, J. Caballero, A. Cunningham, A. Acosta, A. Aitken, A. Tejani, J. Totz, Z. Wang, and W. Shi, "Photo-realistic single image super-resolution using a generative adversarial network," in *2017 IEEE Conference on Computer Vision and Pattern Recognition (CVPR)*, pp. 105–114, Los Alamitos, CA, USA, jul 2017 (IEEE Computer Society), doi:10.1109/CVPR.2017.19, URL https://doi.ieeecomputersociety.org/10.1109/CVPR.2017.19.

8. I. Goodfellow, J. Pouget-Abadie, M. Mirza, B. Xu, D. Warde-Farley, S. Ozair, A. Courville, and Y. Bengio, "Generative adversarial nets," in Z. Ghahramani, M. Welling, C. Cortes, N. Lawrence, and K. Weinberger, eds., *Advances in Neural Information Processing Systems*, volume 27 (Curran Associates, Inc., 2014), URL https://proceedings.neurips.cc/paper_files/paper/2014/file/5ca3e9b122f61f8f06494c97b1afccf3-Paper.pdf.

9. L. Metz, B. Poole, D. Pfau, and J. Sohl-Dickstein, "Unrolled generative adversarial networks," in *5th International Conference on Learning Representations, ICLR 2017, Toulon, France, April 24-26, 2017, Conference Track Proceedings* (OpenReview.net, 2017), URL https://openreview.net/forum?id=BydrOIcle.

10. M. Arjovsky, S. Chintala, and L. Bottou, "Wasserstein generative adversarial networks," in *International Conference on Machine Learning* (2017).

11. I. Gulrajani, F. Ahmed, M. Arjovsky, V. Dumoulin, and A. C. Courville, "Improved training of wasserstein gans," in I. Guyon, U. V. Luxburg, S. Bengio, H. Wallach, R. Fergus, S. Vishwanathan, and R. Garnett, eds., *Advances in Neural Information Processing Systems*, volume 30 (Curran Associates, Inc., 2017), URL https://proceedings.neurips.cc/paper_files/paper/2017/file/892c3b1c6dccd52936e27cbd0ff683d6-Paper.pdf.

12. B. Lewis, T. Scarnati, E. Sudkamp, J. Nehrbass, S. Rosencrantz, and E. Zelnio, "A SAR dataset for ATR development: the Synthetic and Measured Paired Labeled Experiment (SAMPLE)," in E. Zelnio and F. D. Garber, eds., *Algorithms for Synthetic Aperture Radar Imagery XXVI*, volume 10987, p. 109870H (International Society for Optics and Photonics, SPIE, 2019), doi:10.1117/12.2523460, URL https://doi.org/10.1117/12.2523460.

13. H. F. Alqadah and M. J. Burfeindt, "Bistatic aperture completion via untrained fourier convolutional networks," in *2021 International Conference on Electromagnetics in Advanced Applications (ICEAA)*, pp. 377–377 (2021), doi:10.1109/ICEAA52647.2021.9539726.

14. Y. LeCun and C. Cortes, "MNIST handwritten digit database (2010), URL http://yann.lecun.com/exdb/mnist/.